J. Fluid Mech. (2000), *vol.* 408, *pp.* 121–147. Printed in the United Kingdom

Stability boundaries of roll and square convection in binary fluid mixtures with positive separation ratio

By B. HUKE, M. LÜCKE, P. BÜCHEL AND CH. JUNG

Institut für Theoretische Physik, Universität des Saarlandes,
Postfach 151150, D-66041 Saarbrücken, Germany

(Received 29 March 1999 and in revised form 17 September 1999)

Rayleigh–Bénard convection in horizontal layers of binary fluid mixtures heated from below with realistic horizontal boundary conditions is studied theoretically using multi-mode Galerkin expansions. For positive separation ratios the main difference between the mixtures and pure fluids lies in the existence of stable three-dimensional patterns near onset in a wide range of the parameter space. We evaluated the stationary solutions of roll, crossroll, and square convection and we determined the location of the stability boundaries for many parameter combinations thereby obtaining the Busse balloon for roll and square patterns.

1. Introduction

Convection in binary miscible fluids like ethanol–water, ^{3}He–^{4}He, or various gas mixtures shows a rich spectrum of pattern formation behaviour (see e.g. Platten & Legros 1984; Cross & Hohenberg 1993; Lücke *et al.* 1998 for a review). The spatiotemporal properties of convection in mixtures are more complex than those of one-component fluids due to the influence of Soret-sustained concentration gradients. The structural dynamics of the concentration distribution in mixtures results from an interplay between three competing mechanisms: nonlinear advection and mixing, weak solutal diffusion, and the Soret effect. The latter generates and sustains concentration gradients in (linear) response to local temperature gradients. Without Soret coupling, i.e. for vanishing separation ratio $\psi = 0$, any concentration fluctuation diffuses away. For $\psi \neq 0$, however, the externally imposed vertical temperature difference across the fluid layer sustains via the Soret effect concentration variations against the action of advective mixing and diffusive dissipation.

The concentration field changes the advective properties of mixtures via solutal buoyancy forces that enter into the momentum balance of the fluid. Thus, a concentration fluctuation directly influences the flow which in turn changes and mixes the concentration. In binary *liquids*, this nonlinear feedback is only weakly damped by diffusive homogenization so that the concentration distribution shows anharmonic and boundary layer structures. Furthermore, it is ultimately this feedback that causes right at onset convection patterns that cannot be seen there in pure fluids. Examples that occur, depending on parameters, are travelling waves of roll structures, standing wave oscillations, and stationary squares. In addition mixtures show very interesting secondary structures close to onset: spatially localized travelling wave states, stationary crossrolls, and oscillations between squares and rolls or crossrolls can be seen

for different parameter combinations. Note that all of the aforementioned patterns are Soret induced by the concentration field – they disappear in the pure fluid limit, $\psi \to 0$, when the Soret coupling to the concentration field is switched off.

In this paper we are concerned with the case of a positive Soret effect, $\psi > 0$, which causes the heavier (lighter) component of the mixture to be driven towards lower (higher) temperature regions. Therefore, heating a mixture with $\psi > 0$ from below establishes a stronger density gradient as in a pure fluid. The solutal contribution to the buoyancy increases the thermal destabilization of the fluid layer and convection starts at smaller temperature differences compared to a pure fluid. One commonly denotes the thermal driving regime with Rayleigh numbers R below the threshold R_c^0 of pure fluids as the Soret regime and the regime above R_c^0 as the Rayleigh region (Moses & Steinberg 1991). As a crude rule of thumb one can say that in the Soret region, $R < R_c^0$, square patterns are often observed in mixtures, whereas in the Rayleigh region stable rolls are found.

There have been only a few theoretical investigations aimed at explaining the transition scenario between squares at smaller R and rolls at larger R (Clune & Knobloch 1992; Müller & Lücke 1988). Recently we have elucidated this transition for a fixed wavenumber (Jung, Huke & Lücke 1998). In this paper we compare the properties of square, roll, and CR patterns and we present a comprehensive linear stability analysis of rolls and a more restricted one for squares. We elucidate how the stability boundaries of rolls that have been determined by Busse and coworkers (Busse 1967; Bolton, Clever & Busse 1985; Clever & Busse 1990) for pure fluid convection are modified by taking into account the influence of the concentration field in mixtures. We present for the first time a full numerical investigation of the stability behaviour of rolls and squares and present the stability balloons of these patterns in the (k, r)-plane for a wide range of fluid parameters.

The paper is organized as follows. In § 2 we describe briefly the basics of convection in binary fluids and we explain the application of the Galerkin method to this particular system. In § 3 we describe and compare the stationary solutions for rolls, crossrolls, and squares. In § 4 the Galerkin method is used for the linear stability analysis of roll and square patterns. We conclude in § 5 with a summary of our results.

2. Mathematical foundations

In this paper we investigate convection in horizontal binary fluid layers confined between perfectly heat conducting, rigid, impermeable plates. Since the system and its basic equations are well known (Landau & Lifshitz 1966; Platten & Legros 1984), we summarize in § 2.1 only the necessary formulas for our investigation. Then we present relevant details related to the application of the Galerkin expansion technique to this system.

2.1. *System and basic equations*

We consider a horizontal layer of a binary fluid mixture of thickness d in a homogeneous gravitational field, $\boldsymbol{g} = -g\,\boldsymbol{e}_z$. A vertical temperature gradient is imposed by fixing the temperature

$$T = T_0 \pm \frac{\Delta T}{2} \quad \text{at } z = \mp\frac{d}{2}, \tag{2.1}$$

e.g. via highly conducting plates in experiments. Here we consider the plates to be infinitely extended, rigid, and impermeable.

Convection is described in terms of the fields of velocity $\boldsymbol{u} = (u, v, w)$, temperature T, mass concentration C of the lighter component, total mass density ρ, and pressure. In the balance equations connecting these fields we scale lengths and positions by d, time by the vertical thermal diffusion time d^2/κ, temperature by $\nu\kappa/\alpha g d^3$, concentration by $\nu\kappa/\beta g d^3$, and pressure by $\rho_0\kappa^2/d^2$. Here ρ_0 is the mean density, κ the thermal diffusivity, ν the kinematic viscosity, and α and β are thermal and solutal expansion coefficients, respectively. Using the Oberbeck–Boussinesq approximation the balance equations read (Platten & Legros 1984; Hort, Linz & Lücke 1992)

$$\nabla \cdot \boldsymbol{u} = 0, \tag{2.2a}$$

$$(\partial_t + \boldsymbol{u} \cdot \nabla)\boldsymbol{u} = -\nabla p + \sigma[(\theta + c)\,\boldsymbol{e}_z + \nabla^2 \boldsymbol{u}], \tag{2.2b}$$

$$(\partial_t + \boldsymbol{u} \cdot \nabla)\theta = Rw + \nabla^2\theta, \tag{2.2c}$$

$$(\partial_t + \boldsymbol{u} \cdot \nabla)c = R\,\psi\, w + L(\nabla^2 c - \psi\nabla^2\theta). \tag{2.2d}$$

Here θ, c, and p are the reduced deviations of temperature, concentration, and pressure, respectively, from the conductive profiles.

The Lewis number L is the ratio of the concentration diffusivity D to the thermal diffusivity κ, therefore measuring the velocity of concentration diffusion. The Prandtl number σ is the ratio of the momentum diffusivity ν and κ:

$$L = \frac{D}{\kappa}, \qquad \sigma = \frac{\nu}{\kappa}. \tag{2.3}$$

The Rayleigh number R measures the thermal driving and the separation ratio ψ measures the strength of the Soret coupling between temperature and concentration fields

$$R = \frac{\alpha g d^3 \Delta T}{\nu\kappa}, \qquad \psi = -\frac{\beta}{\alpha}\frac{k_T}{T_0}. \tag{2.4}$$

Here T_0 is the mean temperature and k_T is the thermal diffusion ratio (Landau & Lifshitz 1966). The driving forces entering into the momentum balance equation (2.2*b*) are pressure gradients and the buoyancy caused by the temperature and concentration dependence of the density.

The off-diagonal term $-L\psi\nabla^2\theta$ and the term $R\psi w$ in the concentration balance equation (2.2*d*) describe the action of the Soret effect, i.e. the generation of concentration currents and concentration gradients by temperature variations. A Soret coupling $\psi > 0$ implies a positive Soret effect. In this case the lighter component of the mixture is driven in the direction of higher temperature thus increasing the density variations.

The Dufour effect, i.e. the driving of temperature currents by concentration variations, is of interest only in gas mixtures (Hort *et al.* 1992). But even there it is often small (Liu & Ahlers 1997).

2.2. *Galerkin method*

To describe three-dimensional patterns with wavenumbers k_x and k_y each field X is expanded as

$$X(x, y, z; t) = \sum_{lmn} X_{lmn}(t)\mathrm{e}^{\mathrm{i}lk_x x}\mathrm{e}^{\mathrm{i}mk_y y} f_n(z). \tag{2.5}$$

Here l and m are integers and the f_n form a complete system of functions that fits the specific boundary condition for the field X at the plates. To find suitable sets of functions f_n we introduce some new fields. First, two scalar fields Φ and Ψ are

defined via

$$\boldsymbol{u} = \nabla \times \nabla \times \Phi \boldsymbol{e}_z + \nabla \times \Psi \boldsymbol{e}_z. \tag{2.6}$$

The structures we want to discuss do not show a horizontal mean flow for mirror symmetry reasons. Then, (2.6) is the most general expression that fulfils the incompressibility condition (2.2*a*) (Clever & Busse 1989). The analysis of mean flow effects in the perturbations in discussed in § 2.4.

Second, instead of c we use the field

$$\zeta = c - \psi\theta \tag{2.7}$$

that allows the impermeability of the horizontal boundaries to be guaranteed in a more convenient way. The diffusive part of the concentration current, driven by concentration gradients as well as by temperature gradients is given by $-L\nabla(c - \psi\theta)$. At the impermeable plates the vertical component of this current vanishes which requires

$$0 = \partial_z (c - \psi\theta) = \partial_z \zeta \quad \text{at } z = \pm 1/2. \tag{2.8}$$

The advective concentration current vanishes at the plates because there $\boldsymbol{u} = 0$. The balance equation for ζ is obtained by combining (2.2*c*) and (2.2*d*).

The boundary conditions for the fields Φ, Ψ, θ, and ζ read

$$\Phi = \partial_z \Phi = \Psi = \theta = \partial_z \zeta = 0 \quad \text{at } z = \pm 1/2. \tag{2.9}$$

To expand the fields Ψ, θ, ζ, and Φ vertically we used different orthonormal sets $f_n(z)$ as follows:

$$\Psi \text{ and } \theta: \qquad f_n(z) = \begin{cases} \sqrt{2}\cos(n\pi z) & n \text{ odd} \\ \sqrt{2}\sin(n\pi z) & n \text{ even,} \end{cases} \tag{2.10a}$$

$$\zeta: \qquad f_n(z) = \begin{cases} 1 & n = 0 \\ \sqrt{2}\sin(n\pi z) & n \text{ odd} \\ \sqrt{2}\cos(n\pi z) & n \neq 0 \text{ even,} \end{cases} \tag{2.10b}$$

$$\Phi: \qquad f_n(z) = \begin{cases} C_{(n+1)/2}(z) & n \text{ odd} \\ S_{n/2}(z) & n \text{ even.} \end{cases} \tag{2.10c}$$

Here C_n and S_n are Chandrasekhar functions (Chandrasekhar 1981).

The balance equations for the new fields are

$$\partial_t \Delta_2 \Psi = \sigma \nabla^2 \Delta_2 \Psi + \{\nabla \times [(\boldsymbol{u} \cdot \nabla)\boldsymbol{u}]\}_z, \tag{2.11a}$$

$$\partial_t \nabla^2 \Delta_2 \Phi = \sigma\{\nabla^4 \Delta_2 \Phi - \Delta_2[(1+\psi)\theta + \zeta]\} - \{\nabla \times \nabla \times [(\boldsymbol{u} \cdot \nabla)\boldsymbol{u}]\}_z, \tag{2.11b}$$

$$(\partial_t + \boldsymbol{u} \cdot \nabla)\theta = -R\Delta_2 \Phi + \nabla^2 \theta, \tag{2.11c}$$

$$(\partial_t + \boldsymbol{u} \cdot \nabla)\zeta = L\nabla^2 \zeta - \psi \nabla^2 \theta. \tag{2.11d}$$

Here $\Delta_2 = \partial_x^2 + \partial_y^2$.

By inserting the ansatz (2.5) for each field into the balance equations and projecting them onto the basic functions one gets a nonlinear algebraic system of equations of the form

$$A_{\kappa\mu} \partial_t X_\mu = B_{\kappa\mu} X_\mu + C_{\kappa\mu\nu} X_\mu X_\nu. \tag{2.12}$$

For simplicity amplitudes are labelled here by a single Greek index and the summation convention is implied in (2.12) with $A_{\kappa\mu}, B_{\kappa\mu}$, and $C_{\kappa\mu\nu}$ being constant coefficients.

The number of modes has to be truncated to get a finite number of equations as discussed later on. For stationary convection structures the left-hand side of (2.12) vanishes and the solution can be found using a multidimensional Newton method.

2.3. *Symmetries*

Symmetries of convective structures impose conditions on the fields and/or imply relations between different modes of the fields thereby restricting the number of independent modes that are necessary to describe the patterns. For example, to describe two-dimensional roll patterns with $k_x = k$, $k_y = 0$ that do not depend on y, all amplitudes with $m \neq 0$ are set to zero in (2.5). On the other hand, square patterns are characterized by $k_x = k_y = k$ and $X_{lmn} = \pm X_{mln}$. But we also investigate three-dimensional crossroll patterns with $k_x = k_y = k$ for which, however, $X_{lmn} \neq \pm X_{mln}$.

2.3.1. *Stationary rolls*

To describe these two-dimensional structures one does not need the Ψ-field. Furthermore, rolls are even in x with an appropriate choice of the plane $x = 0$. As a consequence of this mirror symmetry one has $X_{l0n} = X_{-l0n}$ so that the lateral functions $e^{\pm iklx}$ can be replaced by $\cos(klx)$. In addition the roll pattern is antisymmetric under reflection in the plane $z = 0$ combined with a translation by half a wavelength in the x-direction. This mirror glide symmetry makes half of the amplitudes zero, e.g. all amplitudes Φ_{l0n} where $l + n$ is an odd number.

It is no accident that stationary roll patterns have these symmetries. That they are fulfilled at onset can be shown via a linear stability analysis of the conductive state (Hollinger & Lücke 1995). The subset of modes that obey these symmetries is closed in the sense that these modes do not drive others via nonlinear coupling. Thus, the observed roll solution remains symmetric as long as no symmetry-breaking bifurcation occurs on the stationary roll branch with symmetry-breaking modes becoming linearly unstable. Such instabilities are covered by our stability analysis. Moore, Weiss & Wilkins (1991) have discussed these symmetry-breaking perturbations for free-slip and permeable boundary conditions.

2.3.2. *Stationary squares and crossrolls with $k_x = k_y$*

These have the same symmetry plane at $x = 0$ as rolls and an additional mirror plane at $y = 0$. Furthermore, the squares and crossrolls also have a mirror glide symmetry. Here, however, the symmetry transformation consists of a reflection in the plane $z = 0$ combined with a translation by half a wavelength in the x- *and* y-directions. To describe these three-dimensional patterns the Ψ-field cannot be neglected. We also mention that in contrast to the other fields Ψ is odd in x and y and has positive parity under the mirror glide operation thereby reflecting the symmetries of the velocity field.

For square patterns that are invariant under rotation by 90° in which the x- and y-directions are indistinguishable a further reduction of the number of mode occurs: amplitudes like Φ_{lmn} and Φ_{mln} are the same. This is also true for θ and ζ. Again Ψ is different. Here $\Psi_{lmn} = -\Psi_{mln}$.

2.4. *Stability analysis*

To make a full stability analysis one has to check the stability of the patterns to perturbations with arbitrary wavevector $d\boldsymbol{e}_x + b\boldsymbol{e}_y$. To do so one has to introduce a

Floquet term, writing the perturbation as

$$\delta X(x,y,z;t) = \mathrm{e}^{\mathrm{i}dx+\mathrm{i}by}\mathrm{e}^{st}\sum_{lmn}\delta X_{lmn}\,\mathrm{e}^{\mathrm{i}lk_x x+\mathrm{i}mk_y y}f_n(z). \tag{2.13}$$

Such a perturbation is added to the known solution, the stability of which is to be tested, and inserted into the balance equations. After linearizing and projecting one gets a linear eigenvalue problem of the form

$$sA_{\kappa\mu}\delta X_\mu = B_{\kappa\mu}\delta X_\mu, \tag{2.14}$$

with constant coefficients $A_{\kappa\mu}$ and $B_{\kappa\mu}$. The aforementioned solution, i.e. the convective structure described by it, is stable if every eigenvalue s has a negative real part for every d and b.

The symmetry of the convective pattern discussed above can under some circumstances be used to get separated classes of possible eigenvectors representing the perturbations. That means the eigenvalue problem can be reduced to finding the eigenvalues of two matrices of about half of the size. Because evaluating the eigenvalues of a matrix is an $O(N^3)$-process this always implies a reduction of the computation time.

2.4.1. *Stationary rolls*

To perform the stability analysis of rolls one determines the growth behaviour of perturbations of the form

$$\delta X(x,y,z;t) = \mathrm{e}^{\mathrm{i}dx+\mathrm{i}by}\mathrm{e}^{st}\sum_{ln}\delta X_{l0n}\,\mathrm{e}^{\mathrm{i}lkx}f_n(z). \tag{2.15}$$

Contrary to the roll solutions, their perturbations may contain a mean flow component that is discarded in (2.6). However, our perturbation ansatz (2.15) contains modes like $\delta\Phi_{001}\mathrm{e}^{\mathrm{i}dx+\mathrm{i}by}C_1(z)$ describing a mean flow in the limit $b,d\to 0$, and the equation of motion for $\delta\Phi_{001}$ reduces to two independent equations for the mean flow as they are used e.g. in Clever & Busse (1991). If there is a mean flow in the perturbations, then modes like the $\delta\Phi_{001}$-mode diverge when b,d goes to zero such that the long-wavelength component of the velocity remains finite. However, in the parameter range explored here, the perturbations limiting the stability balloon of rolls have finite b or d and thus no mean flow.

Because of the periodicity of the patterns in x and their mirror symmetry it suffices to consider $d\in[0,k/2]$. In the y-direction, however, all perturbation wavenumbers, say $b\geqslant 0$, have to be investigated.

The linear system of equations (2.15) always separates into two subsystems of perturbations δX_μ that belong to modes with amplitudes X_μ that are antisymmetric (G-perturbations) or symmetric ($\overline{G}$-perturbations) under the mirror glide operation $(x,y,z)\to(x+\lambda/2,y+\lambda/2,-z)$. For example, all perturbations with amplitudes $\delta\Phi_{l0n}$ with even $l+n$ are G-perturbations, and the perturbations with odd $l+n$ are $\overline{G}$-perturbations.

In general the perturbations (2.15) do not have a well-defined symmetry under the mirror glide operation. This is only the case if $d=nk$. If n is even (odd) then the perturbations have the same (opposite) parity as the modes they belong to. Every G-perturbation can be written as a $\overline{G}$-perturbation (and vice versa) by choosing a new $d'=d-k$. Thus the distinction between G- and $\overline{G}$-perturbations is well defined only for fixed d.

It is possible to restrict the stability analysis to *one* set of perturbations by extending

the investigated d-interval to $[0,k]$. Consider for example a $\overline{G}$-perturbation with $d \in \left[0,k/2\right]$. It can just as well be written as a G-perturbation with a new $d' = d - k$ or equivalently $d' = k - d$. Thus one finds all $\overline{G}$-perturbations with $d \in \left[0,k/2\right]$ again as G-perturbations with $d' \in \left[k/2,k\right]$. We will therefore restrict ourselves to the set of perturbations that has negative parity under the mirror glide operation at $d = 0$, i.e. we investigate the G-perturbations in the whole interval $[0,k]$.

In special cases the system of equations can be separated even further. For $d = 0$ the perturbations can be divided into those that are symmetric and those that are antisymmetric under the operation $x \to -x$. Furthermore, if $b = 0$ then the perturbations contain either no or only $\delta\Psi$-amplitudes.

2.4.2. *Stationary squares and crossrolls with $k_x = k_y$*

Because the amount of computational power needed to make a full stability analysis of these three-dimensional structures is too large, we will discuss perturbations only for periodic boundary conditions, i.e. $d = b = 0$. Here again a separation of perturbations is possible into those that change sign or do not under the mirror glide operation.

Furthermore, the stability problem is invariant under $x \to -x$ and $y \to -y$. Thus one can distinguish between perturbations that are even in x and y, odd in x and y, or even in x and odd in y (or equivalently odd in x and even in y). If the perturbations have the same symmetry in both directions one can in the case of squares finally make use of a last symmetry property and separate perturbations that are symmetric or antisymmetric under the exchange of the x- and y-directions. This is not possible for CR patterns because of their lack of the $x \leftrightarrow y$ symmetry.

As we will see in §4.3, the destabilizing perturbations of squares fall into the subclass that is even in x and y, and therefore do not drive a mean flow.

3. Properties of the patterns

Squares, crossrolls, and rolls are realized as stable convection structures somewhere in parameter space. Furthermore, if L is sufficiently small these three patterns appear for fixed L, σ, ψ, and k as global attractors at different Rayleigh numbers (however, crossrolls coexist bistably with oscillations in a small R-interval (Jung *et al.* 1998)). So it is easy to enforce their stable experimental realization successively by increasing the Rayleigh number beyond the onset of convection.

To understand the behaviour of the patterns it is useful to consider the driving region near onset and the Rayleigh region separately. In the pure fluid the critical point is at a Rayleigh number $R_c^0 = R_c(\psi = 0) = 1707.762$ and a wavenumber $k_c^0 = k_c(\psi = 0) = 3.117$ (Chandrasekhar 1981). In the binary mixtures with positive separation ratios that we are dealing with, the critical Rayleigh number is smaller, $R_c(\psi > 0) < R_c^0$, since the solutal contribution to the quiescent state's buoyancy force enhances the latter. Thus a smaller thermal driving, i.e. a smaller Rayleigh number, suffices to reach the critical buoyancy force size for onset of convection. The critical wavenumber is also somewhat lower: $k_c(\psi > 0) < k_c^0$ (Knobloch & Moore 1988).

When presenting our results we shall use the reduced Rayleigh number

$$r = \frac{R}{R_c^0} \tag{3.1}$$

and the reduced distance

$$\epsilon = \frac{R}{R_c} - 1 = \frac{r}{r_c} - 1 \tag{3.2}$$

from threshold $r_c = R_c/R_c^0$.

3.1. *Small-amplitude convection: amplitude equation*

Very close to onset the wavenumber-dependent bifurcation behaviour of rolls and squares can in pure fluids as well as in binary mixtures be described most simply by two coupled cubic amplitude equations of the form

$$\tau_0 \partial_t A = \epsilon A + \xi_0^2 \left(\partial_x - \frac{\mathrm{i}}{2k_c}\partial_y^2\right)^2 A - |A|^2 A - f|B|^2 A, \tag{3.3a}$$

$$\tau_0 \partial_t B = \epsilon B + \xi_0^2 \left(\partial_y - \frac{\mathrm{i}}{2k_c}\partial_x^2\right)^2 B - |B|^2 B - f|A|^2 B. \tag{3.3b}$$

Clune & Knobloch used such equations without the spatial derivative term (Clune & Knobloch 1991). For a review of such amplitude equations and how they are related to the basic equations see, e.g. Cross & Hohenberg (1993).

The amplitudes A and B of the eigenfunctions of the linearized hydrodynamic field equations correspond quite well to the leading amplitudes

$$w_{101} = k^2 \Phi_{101} = k^2 \int \Phi(x,y,z)\, \mathrm{e}^{\mathrm{i}kx}\, C_1(z)\, \mathrm{d}x\, \mathrm{d}y\, \mathrm{d}z, \tag{3.4a}$$

$$w_{011} = k^2 \Phi_{011} = k^2 \int \Phi(x,y,z)\, \mathrm{e}^{\mathrm{i}ky}\, C_1(z)\, \mathrm{d}x\, \mathrm{d}y\, \mathrm{d}z \tag{3.4b}$$

of the vertical velocity field or the corresponding amplitudes of the temperature field.

The two roll solutions of (3.3) are $A = |A_R|\mathrm{e}^{\mathrm{i}(k-k_c)x}, B = 0$ for rolls with wavevector $\boldsymbol{k} = k\boldsymbol{e}_x$ and $A = 0, B = |B_R|\mathrm{e}^{\mathrm{i}(k-k_c)y}$ for rolls with wavevector $\boldsymbol{k} = k\boldsymbol{e}_y$. Squares are described by the solution $A = |A_S|\mathrm{e}^{\mathrm{i}(k-k_c)x}, B = |B_S|\mathrm{e}^{\mathrm{i}(k-k_c)y}$ with $A_S = B_S$. Crossrolls, i.e. solutions with finite $|A| \neq |B|$, do not exist in (3.3).

If $f > -1$, the square solution exists besides the roll solution for ϵ above the neutral stability curve

$$\epsilon_{stab}(k) = \xi_0^2 (k - k_c)^2. \tag{3.5}$$

We will always consider roll patterns with $B_R = 0$ and $A_R \neq 0$. For the roll solutions one has

$$|A_R|^2 = \epsilon - \epsilon_{stab}(k), \tag{3.6}$$

and for squares one finds

$$|A_S|^2 = |B_S|^2 = \frac{\epsilon - \epsilon_{stab}(k)}{1+f} \tag{3.7}$$

so that

$$|A_R|^2 = (1+f)|A_S|^2. \tag{3.8}$$

A stability analysis of the roll and square solutions shows that squares (rolls) are stable (unstable) whenever $|A_R|^2 < 2|A_S|^2$, i.e. for $-1 < f < 1$, and they are unstable (stable) whenever $|A_R|^2 > 2|A_S|^2$.

3.2. *Full Galerkin expansion*

Both square and roll solutions exist for every r above onset $r_c(\psi, L)$ and the mode intensity $|w_{101}|^2$ for rolls is always greater than for squares. Hence the parameter f in the amplitude equation has to be greater than 0 according to (3.8). In figure 1 we

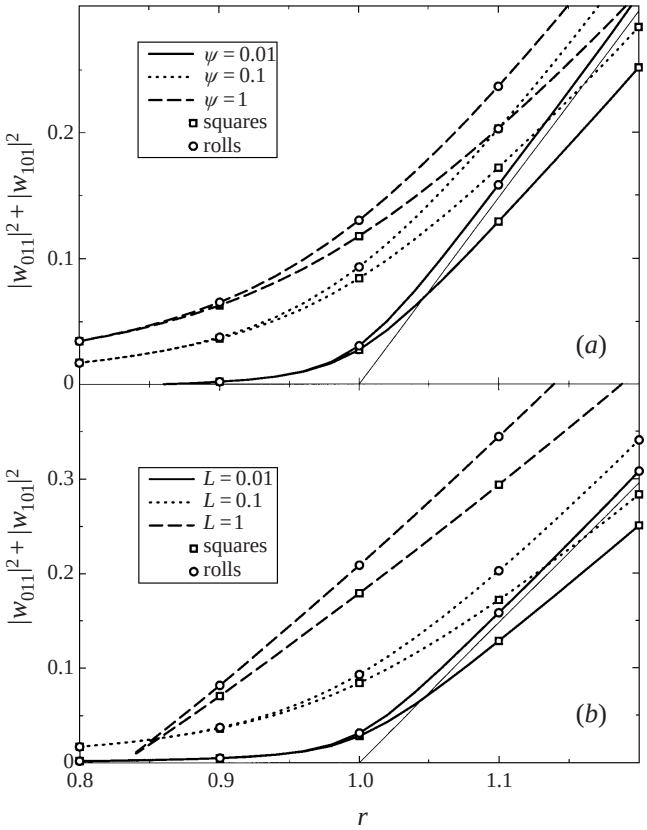

FIGURE 1. Flow intensity of stationary squares and rolls: the contribution $k^2(|\Phi_{101}|^2 + |\Phi_{011}|^2)$ from the leading modes to w^2 versus reduced Rayleigh number. Parameters are $\sigma = 1$, $L = 0.01$ (*a*), and $\psi = 0.08$ (*b*). The thin curves denote the roll solution in pure fluids ($\psi = 0$).

present a plot of the leading contribution $|w_{101}|^2 + |w_{011}|^2$ to the vertical flow intensity w^2 versus r as obtained from the full Galerkin expansion for several parameters.

By comparing our results from the full Galerkin expansion with the amplitude equation approximation we verified that the latter works well near onset $r_c(\psi)$ which in figure 1 lies significantly below 1 – outside the plot range of figure 1. However, at larger r when approaching the Rayleigh regime the amplitude approximation loses its validity: $|A|^2 + |B|^2$ continues to grow linearly with r with its initial slope at onset whereas $|w_{101}|^2 + |w_{011}|^2$ strongly curves upwards in the Rayleigh regime. Furthermore, while $|w^R_{101}|^2 < |w^S_{101}|^2 + |w^S_{011}|^2 = 2|w^S_{101}|^2$ holds close to onset – as required within the amplitude equation approximation for squares to be stable – the full solutions at larger r are such that $|w^R_{101}|^2 > |w^S_{101}|^2 + |w^S_{011}|^2$ without, however, rolls becoming stable, which happens at even higher r.

In the Rayleigh region the amplitudes become comparable with those of the pure fluid. This is because the concentration field gets more and more advectively mixed and equilibrated and therefore loses its influence on the convection. Pure fluid convection, $\psi = 0$, can be described close to onset $r_c(\psi = 0) = 1$ by a cubic amplitude equation. However, the initial slope of w^2 versus r is much greater than for the binary mixtures shown in figure 1 with $\psi > 0$. The transition between the Soret and Rayleigh regions is especially sharp at small L – cf. the bifurcation diagram for $L = 0.01$ in figure 1(*b*). We will observe such behaviour again when we consider the stability of the patterns.

In the r-range investigated in this paper the field amplitudes Φ_{101} and Φ_{011} that are kept in the amplitude equation approximation are also the leading ones in the full Galerkin expansion. To describe only the fixed point solutions it would be sufficient to approximate the velocity field of rolls (squares and crossrolls) by one mode (two modes) only. But this restriction does not suffice when the linear stability is investigated.

Although more than two amplitudes are needed, a good representation is easier to achieve for the velocity field than for the ζ- and θ-fields. For them very many modes are needed if L is small and r is large. This is a region of the parameter space where the concentration field shows narrow boundary layer behaviour which has to be resolved properly. In addition a consistent description of the temperature field then also requires – despite the fact that it is rather smooth – high θ-modes as discussed by Hollinger & Lücke (1998) and Hollinger (1996).

We followed Clever & Busse (1989) when defining our truncation prescription for the Galerkin expansion. We defined a maximal mode index N and neglected all modes X_{lmn} with $|l| + |m| + n > N$. We took the smooth behaviour of the velocity field into account by defining two different indices: N_1 for the Φ- and Ψ-fields and $N_2 = 2N_1$ for the θ- and ζ-fields. For the most anharmonic roll structures at $r \approx 1.5$, $L < 0.01$, and $\psi = 0.15$ that we have investigated expansions up to $N_2 = 40$ were needed. This is much more than for pure fluids, where truncations with $N \leqslant 8$ are sufficient to describe the stability behaviour quantitatively even at large r. Since the structure of squares is somewhat smoother than that of rolls (cf. § 3.4) and since they exist stably only at small r in or near the Soret region, we needed only $N_2 \leqslant 20$ for squares. Also the crossroll structures could be described well with such a truncation near the first bifurcation point at small r, where they behave like squares. But in order also to resolve the crossroll structures close to the second bifurcation point at larger r where the crossroll solution merges into the roll solution (cf. § 3.3) more modes would have been necessary.

3.3. *Bifurcation behaviour of rolls, squares, and crossrolls*

Figure 2 shows a typical bifurcation diagram for a parameter combination where the three stationary patterns can be found. It also contains information on the stability of these patterns. Crossrolls exist only in a finite r-interval. The crossroll solution branches emerge out of the square branch slightly above $r = 1$. At $r \simeq 1.36$ the crossroll solution disappears when, e.g. the amplitude w_{011}^{CR} (downwards pointing triangles in figure 2) becomes zero and the crossroll branch for w_{101}^{CR} (upwards pointing triangles) ends on the roll solution branch w_{101}^{R}.

On the other hand, roll as well as square solutions exist for all $r \geqslant r_c$ of figure 2. Initially at onset the latter are stable and the former are unstable. For the parameters of figure 2 squares lose their stability in a Hopf bifurcation at $r \simeq 1.11$ to oscillations which with increasing r eventually undergo a subharmonic bifurcation cascade that is terminated when the crossroll states have become sufficiently attractive to quench the oscillations. For other parameter combinations, in particular for larger L, there are no oscillations and the squares transfer their stability directly to crossrolls (Jung *et al.* 1998).

3.4. *Structural properties of roll and square fields*

In figure 3 we show the concentration distribution of square convection for two parameter combinations that are representative of liquid and gas mixtures. This plot and the concentration field structure of rolls and squares in a vertical cross-section

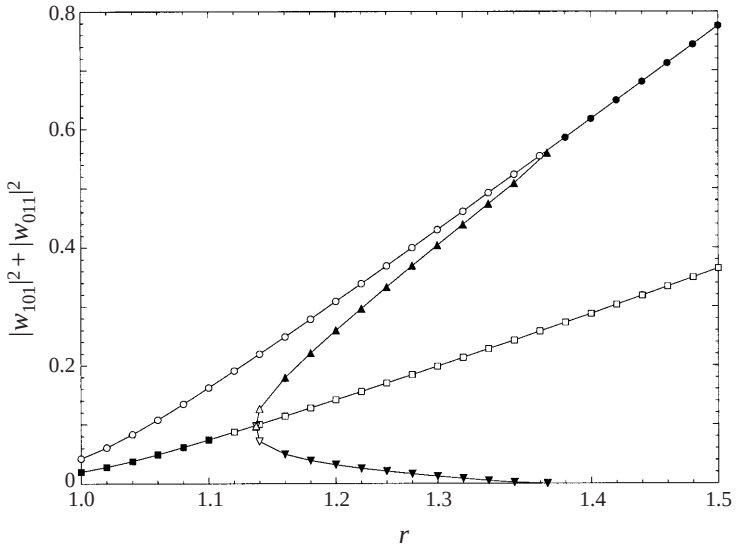

FIGURE 2. Representative bifurcation diagram of stationary patterns. The two most important modes of the velocity field are plotted versus r. Squares, circles, and triangles denote the square, roll, and CR solutions, respectively. Upwards (downwards) pointing triangles refer to, say, $|w_{101}^{CR}|^2$ ($|w_{011}^{CR}|^2$) for CRs with dominant 101 mode. Closed (open) symbols denote stable (unstable) structures. In the interval $1.11 \lesssim r \lesssim 1.15$ the stationary solutions are unstable but an oscillatory solution is stable (Jung *et al.* 1998). Parameters are $L = 0.01$, $\sigma = 10$, $\psi = 0.15$, and $k = k_c^0$. To get a consistent bifurcation diagram all solutions had to be calculated with the same truncation level $N_2 = 16$ (see text). However, this is not sufficient to describe rolls quantitatively.

show a characteristic boundary layer and plume behaviour at small L. Such structures occur when advective mixing is large compared to diffusion in the bulk of the fluid. Consequently the boundary layers and plumes are more pronounced in rolls than in squares since $w_R^2 > w_S^2$ as discussed in § 3.2. Thus squares with their broader boundary layers are much smoother structures than rolls at the same parameters.

The practically harmonic velocity and temperature fields are not shown. For squares they resemble the fields of a linear superposition of two perpendicular sets of rolls.

The Nusselt number N is roughly the same for rolls and squares. Close to onset

$$N - 1 \propto |w_{101}|^2 + |w_{011}|^2, \tag{3.9}$$

and the stable structure has the higher Nusselt number there, i.e. $N_R < N_S$ in accordance with the inequalities of § 3.1 predicted by the amplitude equation. Further away from onset, however, one has $N_S < N_R$ thus reflecting the magnitude relations of w^2 discussed in § 3.2.

In figure 4 we show the mixing parameter

$$M = \frac{\sqrt{\langle \delta C^2 \rangle}}{\sqrt{\langle \delta C_{cond}^2 \rangle}}. \tag{3.10}$$

It is defined by the mean square of the deviation, $\delta C = C - C_0$, of the concentration from the spatial mean, $C_0 = \langle C \rangle$, reduced by the concentration variance in the quiescent conductive state. Note that M is nearly the same for the very different concentration fields of rolls and squares, if L is not too large (figure 4).

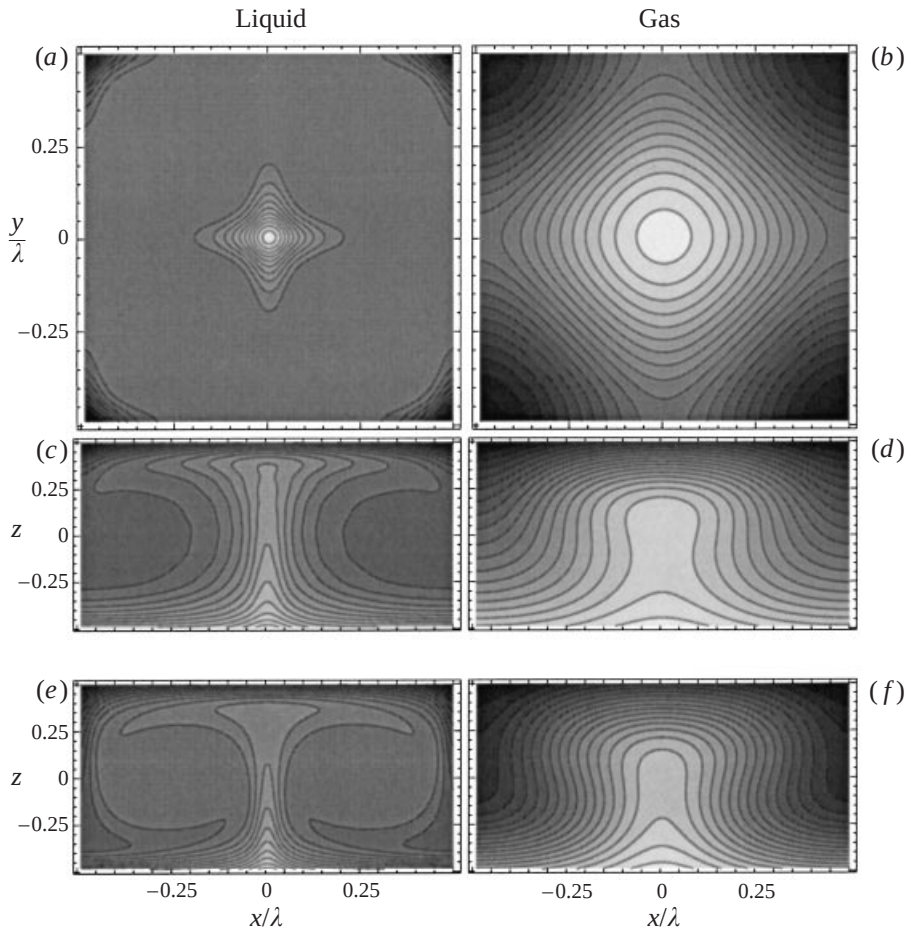

FIGURE 3. Structural properties of square (*a–d*) and roll (*e, f*) convection for representative liquid parameters ($L = 0.01$, $\sigma = 10$, left column) and gas parameters ($L = \sigma = 1$, right column) at $r = 1, \psi = 0.15$. In (a, b) the concentration distribution of squares at mid-height, $z = 0$, is shown. In (*c–f*) we show the concentration distribution in a vertical cross-section at $y = 0$. The largest vertical upflow is at $x = y = 0$.

4. Linear stability analysis of rolls and squares

4.1. *Instability mechanisms of rolls*

The stability boundaries of roll patterns in pure fluids have been known since the pioneering work of Busse (1978). At small Rayleigh numbers there exist five different instability mechanisms giving rise to five different stability boundaries that limit the region of stable rolls in the (R, k, σ)-parameter space. At small Prandtl numbers the Eckhaus (EC), the skewed varicose (SV), and the oscillatory mechanism (OS) are the important instabilities (Clever & Busse 1990). At higher Prandtl numbers the zigzag (ZZ) and the crossroll (CR) mechanisms dominate (Busse 1967). Properties and symmetries of these perturbations are discussed in Bolton *et al.* (1985). All these five instabilities of roll patterns can also be found in binary mixtures.

In pure fluids and binary mixtures there always exist perturbations of the form (2.15) with $b = d = 0$ to which a roll pattern is only marginally stable. Such a perturbation has no Ψ-component and is odd in x. It reflects just an infinitesimal

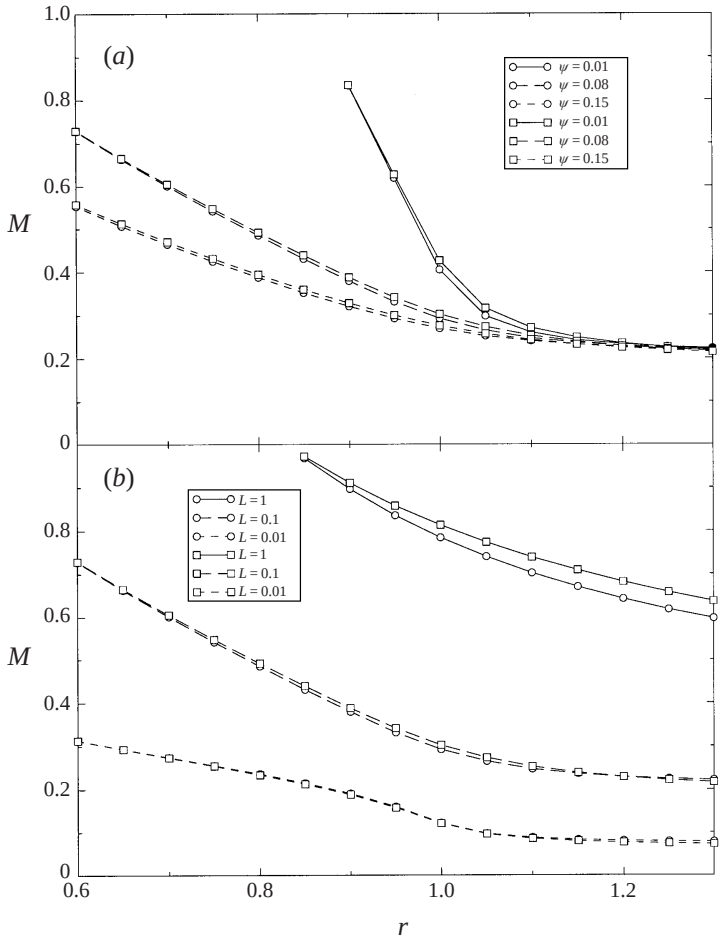

FIGURE 4. Mixing parameter M (3.10) versus r for rolls (circles) and squares (squares). Parameters are $k = 3.117$, $\sigma = 1$, and $L = 0.1$ (a), $\psi = 0.08$ (b).

shift of the whole pattern in the x-direction. Therefore such a perturbation has an eigenvalue $s = 0$. For later discussion we point out here that this particular eigenvalue is connected to nearly all instabilities: the perturbations causing them and the associated eigenvalues evolve smoothly into the lateral shift when one moves in the (d, b)-plane from the d, b coordinates that locate the instability at the origin $d = b = 0$.

In the remainder of this subsection we will briefly characterize the properties of the aforementioned five perturbations before presenting our results of the stability analyses for rolls in § 4.2 and for squares in § 4.3. We begin with the three types (EC, ZZ, and CR) that touch the critical point $\epsilon = 0$, $k = k_c$ and that also exist within the two coupled amplitude equations (3.3a, b).

4.1.1. *Eckhaus instability*

Perturbations of the Eckhaus type are most critical at $b = 0$ and have no Ψ-component. Thus they can be described as purely two-dimensional. The EC instability tends to establish a new set of rolls with a better wavenumber in the direction of the wave vector of the unstable roll pattern. Within the amplitude equations EC

perturbations can be represented as variations of the A-amplitude that depend only on x. Instability occurs here for ϵ and k such that $\epsilon_{stab}(k) < \epsilon < \epsilon_{EC}(k) = 3\,\epsilon_{stab}(k)$. As $d \to 0$ the EC perturbations reduce to the lateral shift both in the amplitude equation approximation and in the full hydrodynamic equations. For symmetry reasons $s \sim d^2$ near $d = 0$. In the case of EC instability (stability) there is a minimum (maximum) of s at $d = 0$. It is therefore sufficient to investigate the pattern at a single point on the d-axis near $d = 0$ numerically in order to determine the stability behaviour to EC perturbations. But to find the most critical value of d an evaluation and interpolation of s along the d-axis is necessary.

4.1.2. *Zigzag instability*

Zigzag perturbations have $d = 0$ and fall into the subclass of perturbations that are odd in x. In the amplitude equations they appear as y-dependent perturbations in the A-amplitude. They cause the growth of a new set of rolls that always has a greater wavenumber than the original set. Consequently they confine the region of stable rolls on the small-k side. The amplitude equations predict a ZZ instability for all $k < k_c$. Like EC perturbations the ZZ instability reduces to the lateral shift when $b \to 0$ and the question of stability can be answered at a single point near $d = b = 0$.

4.1.3. *Crossroll instability*

This occurs when roll-like perturbations perpendicular to the existing pattern can grow. In the amplitude equations (3.3a, b) they are described as perturbations in the amplitude B when A describes the stationary roll pattern. Rolls are CR-unstable for $\epsilon_{stab}(k) < \epsilon < \epsilon_{CR}(k) = f/(f-1)\,\epsilon_{stab}(k)$ when $f > 1$. In this case $\epsilon_{CR}(k)$ can be above or below the Eckhaus boundary $\epsilon_{EC}(k) = 3\,\epsilon_{stab}(k)$ depending on whether $f < \frac{3}{2}$ or not. However, if $f < 1$ (which is the case when squares are stable, cf. § 3.1) then rolls are CR-unstable for all $\epsilon > \epsilon_{stab}(k)$ within the amplitude equation approximation (3.3a, b). Note that the case $f < 1$ does not occur in pure fluids but it can occur in binary mixtures when squares are stable at onset.

In the multi-mode Galerkin expansion the leading mode in the velocity field of the CR perturbation has the form

$$\delta\Phi_{001}\mathrm{e}^{\mathrm{i}by}C_1(z), \tag{4.1}$$

where near the critical point $b \approx k_c$. This is a mode of the $\overline{G}$ class of perturbations that are symmetric under the mirror glide operation as discussed in § 2.4.1. Being a member of the $\overline{G}$ class this perturbation cannot be connected smoothly in the (d, b)-plane to EC or ZZ perturbations since the latter belong to the G class of perturbations that are antisymmetric under the mirror glide operation. Since we decided to transform all perturbations into the G class by a shift $d' = d - k$ as explained in § 2.4.1 we have to rewrite the above CR perturbation (4.1) in the form

$$\delta\Phi_{-101}\mathrm{e}^{\mathrm{i}(d-k)x+\mathrm{i}by}C_1(z). \tag{4.2}$$

Writing the CR perturbations in this form one finds again that the corresponding eigenvalue is connected to the eigenvalue of the lateral shift, only taken at a different $d = k$.

Since the CR instability does not occur at arbitrarily small b one therefore has to test several values of b and then apply an interpolation procedure.

4.1.4. *Skewed varicose instability*

This instability is not captured by the simple amplitude equations. The SV boundary confines the stability balloon on the large-k side. When crossing this boundary the

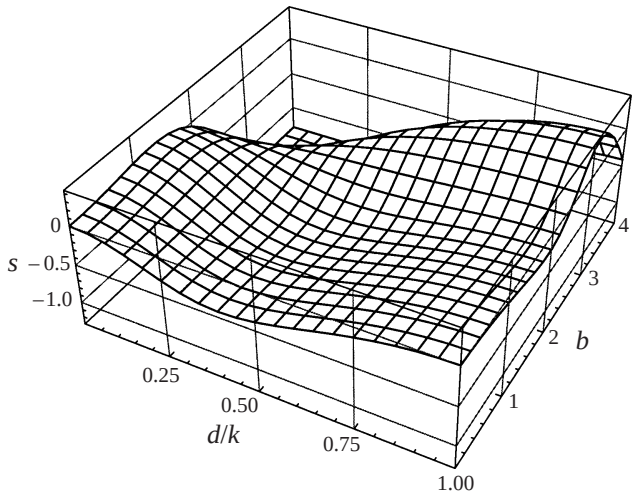

FIGURE 5. Variation of a representative eigenvalue s as a function of perturbation wavenumbers d, b. The positive maximum at $d = 0$ and $b \approx 1.5$ ($d = k$ and $b \approx 3.0$) implies ZZ (CR) instability. Parameters are $r = 1$, $k = 2.7$, $\sigma = 10$, $\psi = 0.08$, and $L = 0.1$.

perturbation tends to replace the original set of rolls by a new set with smaller wavenumber. The eigenvalue has its maximum at $d \neq 0$ and $b \neq 0$. The SV instability also reduces to a lateral shift at $d, b \to 0$ and can be found at infinitesimal small b and d. To find the SV stability boundary of rolls one has to find the maximum of the eigenvalue on a line between the d- and b-axes near the origin.

4.1.5. *Oscillatory instability*

The oscillatory instability is the only instability with complex eigenvalues at small r. The perturbation is most critical at $d = 0$ and finite b. It is even in x. The pair of complex conjugate eigenvalues undergoes a collision near $b = 0$ and generates two real eigenvalues. One of these stationary perturbations transforms into the lateral shift. The real eigenvalues are negative (if the pattern is stable to ZZ perturbations), so the search for the OS instability requires an evaluation and interpolation along the b-axis as for the CR instability.

4.2. *Stability boundaries of rolls*

We saw that the EC, ZZ, CR, SV, and one eigenvalue of the OS instability are connected to the lateral shift at $b = d = 0$. Figure 5 shows an example of the most dangerous eigenvalue in the (d, b)-plane. Along the d-axis the value of s decreases from $s = 0$ at the origin. The pattern is therefore EC stable. The maxima at $d = 0$ and $d = k$ show that it is unstable to ZZ and CR perturbations. An oscillatory instability does not occur here for these parameters since the eigenvalue is always real. There is also no SV instability; this would cause a relative maximum between the d- and b-axes.

Besides the perturbation at $d = b = 0$ which describes a lateral shift in all fields there is another important location in wavenumber space that is of relevance for concentration field perturbations and which thus is specific to binary mixtures. It lies at $d = k$, $b = 0$ and describes a change of the mean concentration. This is most easily understood by transforming this perturbation from the G class into the $\overline{G}$ class where it then occurs at $d = b = 0$. Here it consists of one single mode $\delta\zeta_{000}$. This mode is

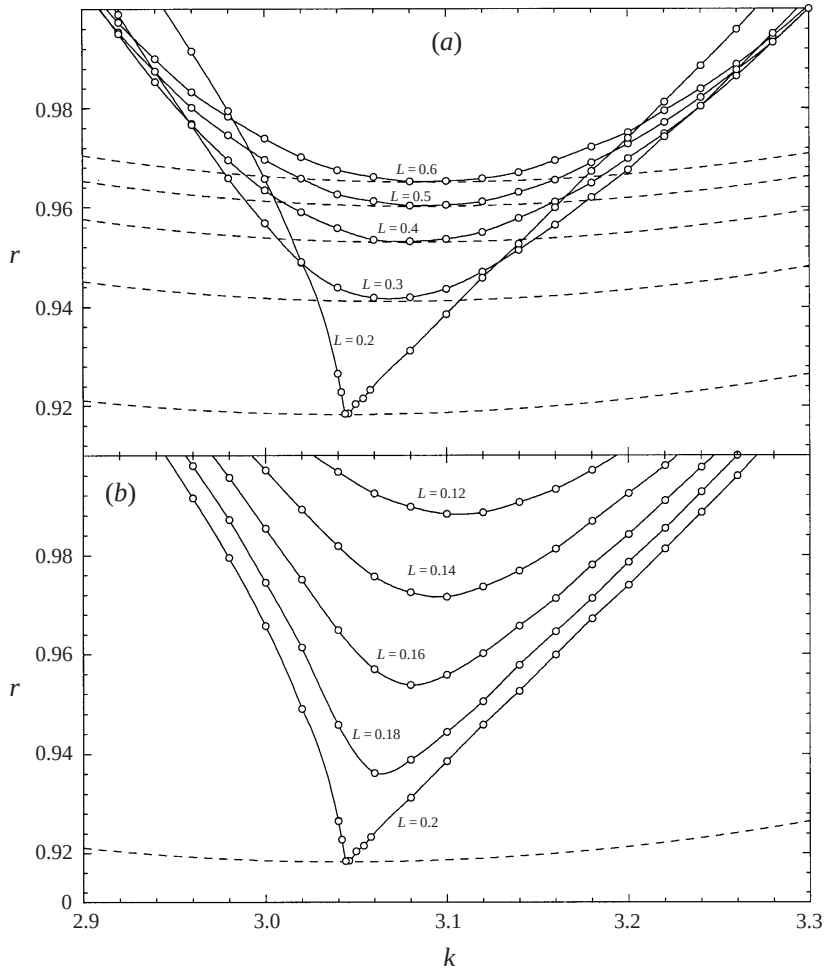

FIGURE 6. CR instability boundaries (solid lines) of rolls in the Soret region for $\sigma = 10$, $\psi = 0.01$ and several values of L. Rolls are stable to CR-perturbations above the solid lines. (*a*) For $L \geqslant 0.2$ the CR boundaries touch the neutral curve (dashed lines) in the critical point. (*b*) For $L < 0.2$ the neutral curve goes further down (not shown) and is disconnected from the CR boundaries. Then rolls are not stable at the critical point anymore.

constant in the fluid layer and describes a change in the average concentration. But since only derivatives of the ζ-field appear in the balance equations such a mode has no influence so that $s = 0$. The reason why this mode has to be taken into account is that for d, $b \neq 0$ it describes a long-wavelength perturbation $\delta\zeta_{000}\mathrm{e}^{\mathrm{i}dx+\mathrm{i}by}$ that is of physical importance. Because the average concentration is fixed, a divergence in the $\delta\zeta_{000}$-amplitude (as in $\delta\Phi_{001}$ for mean flow) cannot occur when approaching $b, d = 0$. While the eigenvalue of the CR perturbation is connected to the above described zero eigenvalue the CR instability always occurs at finite b. Only far in the unstable region does the CR eigenvalue become positive at arbitrary small b. However, we found no roll instability to occur directly near this point whereas EC, ZZ, and SV instabilities are realized near the origin $d = b = 0$ as modifications of the lateral shift.

Figure 6 shows the CR instability boundaries of rolls in the full Galerkin model in a parameter interval where an exchange of stability between rolls and squares at

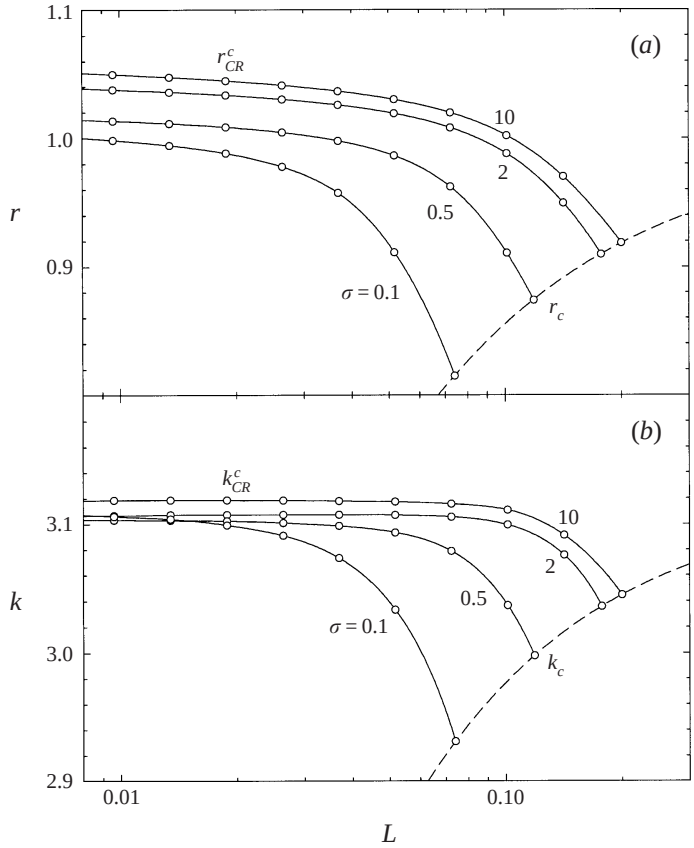

FIGURE 7. (*a*) The minimum of the CR-boundary r^c_{CR} denoting the smallest r where CR-stable rolls exist as a function of L for several values of σ and $\psi = 0.01$. (*b*) The corresponding wavenumbers k^c_{CR}.

onset is predicted in Clune & Knobloch (1991). One sees that the curvature of the CR boundary at the critical point diverges – as is also predicted by the amplitude equation (3.3*a*, *b*) for $f = 1$ – when this exchange occurs. For the parameters $\sigma = 10, \psi = 0.01$ of figure 6 the exchange occurs at $L = 0.2$. On decreasing L below this value the neutral stability curve (dashed line in figure 6) drops further down in r (not shown in figure 6*b*) while the CR instability boundary moves up in r. The r-range between these two curves locates stable squares. In such a situation where squares are stable at onset the amplitude equations predict rolls to be CR-unstable everywhere while in the full equations rolls become stable to CR-perturbations above the solid lines in figure 6.

The rolls could still be unstable there to other perturbations but we found the minimum of the CR boundary always to be the minimal Rayleigh number for stable rolls to exist. To know the location, r^c_{CR}, of this minimum of the CR boundary for several parameters is therefore of interest. We have determined r^c_{CR} and the associated wavenumber k^c_{CR} of the most dangerous CR perturbation for $\psi = 0.01$ and $\psi = 0.15$ and presented the results in figures 7 and 8, respectively. They show that rolls are CR-unstable at onset, r_c (dashed lined in figures 7*a* and 8*a*), for small L and large σ. However, for larger L, being typical for gas mixtures, rolls are stable at the critical point.

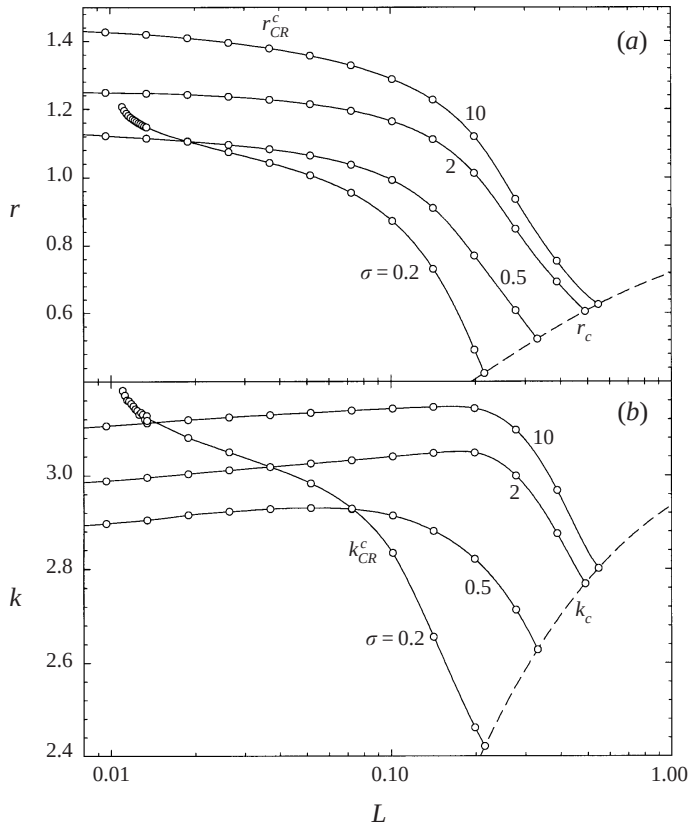

FIGURE 8. Same as figure 7, but for $\psi = 0.15$.

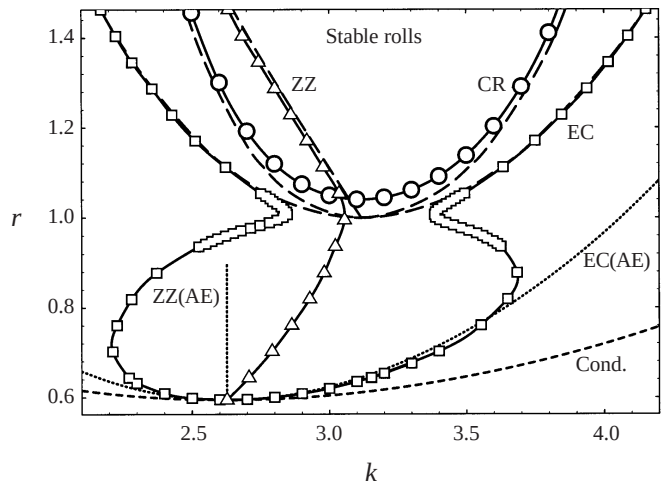

FIGURE 9. Stability boundaries of rolls. Solid lines with open symbols refer to a mixture with $\sigma = 7$, $\psi = 0.01$, and $L = 0.025$. The corresponding boundaries in a pure fluid with $\sigma = 7$ are the long-dashed curves. Dotted curves labelled EC(AE) and ZZ(AE) are the predictions of the cubic amplitude equations for the EC and ZZ boundaries of the mixture, respectively. The conductive state, labelled Cond., is stable below the short-dashed curve

At $\psi = 0.15$ the minimum r^c_{CR} of the CR boundary and its wavenumber location k^c_{CR} strongly increase for small σ and L, cf. the small-L variation of the respective curves at $\sigma = 0.2$ in figure 8(a,b); r^c_{CR} seems to diverge here, but a detailed inspection shows that this is not true. The two branches of the CR boundary meet again at higher r near the apparent divergence. They limit in the (k,r)-plane an oval region of CR-stable rolls from below and also *above*. (The upper part of this region can be unstable to OS-perturbations, though.) On reducing L r^c_{CR} remains finite but the oval region gets smaller until the region of stable rolls vanishes. The experimental observation of this behaviour might be difficult because it occurs in a region of the parameter space that is not reached by ordinary fluid mixtures.

We also investigated the behaviour of b^c_{CR}, the wavenumber of the critical perturbation at (k^c_{CR}, r^c_{CR}). Only in the Rayleigh region are the values of k^c_{CR} and b^c_{CR} near $k_c = 3.117$. But in general $k^c_{CR} \neq b^c_{CR}$. The *linear* analysis thus gives a hint of the existence of patterns with $k_x \neq k_y$ in the Soret region.

We have calculated all stability boundaries at small r for different values of L, ψ, and σ. Concerning the stability behaviour of the roll structures one sees that in the Rayleigh region, $r \gtrsim 1$, where the concentration field is nearly uniform the binary mixture behaves like a pure fluid. And the transition between the Soret and Rayleigh regions is very sharp at small L and ψ. An example of such behaviour is given in figure 9. Here only the EC, CR, and ZZ boundaries are of importance. In the Rayleigh region $r \gtrsim 1$ of figure 9 the CR, ZZ, and EC boundaries of the mixture (full lines with circles, triangles, and squares, respectively) are lying close to the corresponding boundaries of the pure fluid (long-dashed lines). Note in particular the vase-like form of the EC boundary $r_{EC}(k)$ and the dent in the ZZ boundary $r_{ZZ}(k)$: close to onset ($r_c \simeq 0.6, k_c \simeq 2.6$ in figure 9), i.e. in the Soret regime, $r_{EC}(k)$ opens up parabolically and $r_{ZZ}(k)$ comes out of the critical point linearly with positive slope. However, in the crossover range $r \sim 1$ between the Soret and Rayleigh regimes the curve $r_{EC}(k)$ pinches inwards and develops a waist so that in the Rayleigh regime it follows the parabolic shape of the EC curve of the pure fluid that starts at $k^0_c \simeq 3.1, r^0_c = 1$. Similarly, in the crossover range $r_{ZZ}(k)$ bends towards small k to follow the ZZ boundary of the pure fluid that has negative slope.

Figures 10–12 show that this sharp transition between the Soret and Rayleigh regions that causes the vase-like structure of the EC boundary and the sharp bend of the ZZ boundary does not occur when L is greater. For $L = 0.01$ and $\psi \geqslant 0.08$ the critical point lies at $k = 0$. In this case the amplitude equations are not applicable. We found the ZZ boundary and the left-hand EC branch to go to $r = \infty$ at small k. But the right-hand EC branch does still meet the critical point.

At low Prandtl numbers the roll solutions have a finite region of stability but their basin attraction seems to be very small since typically spiral defect chaos is observed here in experiments (Liu & Ahlers 1996). But it has been shown that rolls could also be observed with special experimental procedures (Cakmur *et al.* 1997).

We tried to find laws that connect the position of the boundaries and the fixed point solutions. We found no simple connection between these for CR, ZZ and SV. But the OS boundary for fixed σ seems to be independent of L and ψ in the plane of k and the convection amplitude w_{101} instead of in the (k,r)-plane (figure 13).

For the EC boundary a more complicated procedure is needed. We define an effective control parameter by linear interpolation of the values for the convection amplitudes

$$\frac{\partial w^2_{101}}{\partial r}\,\epsilon_{eff}(r) = w^2_{101}, \tag{4.3}$$

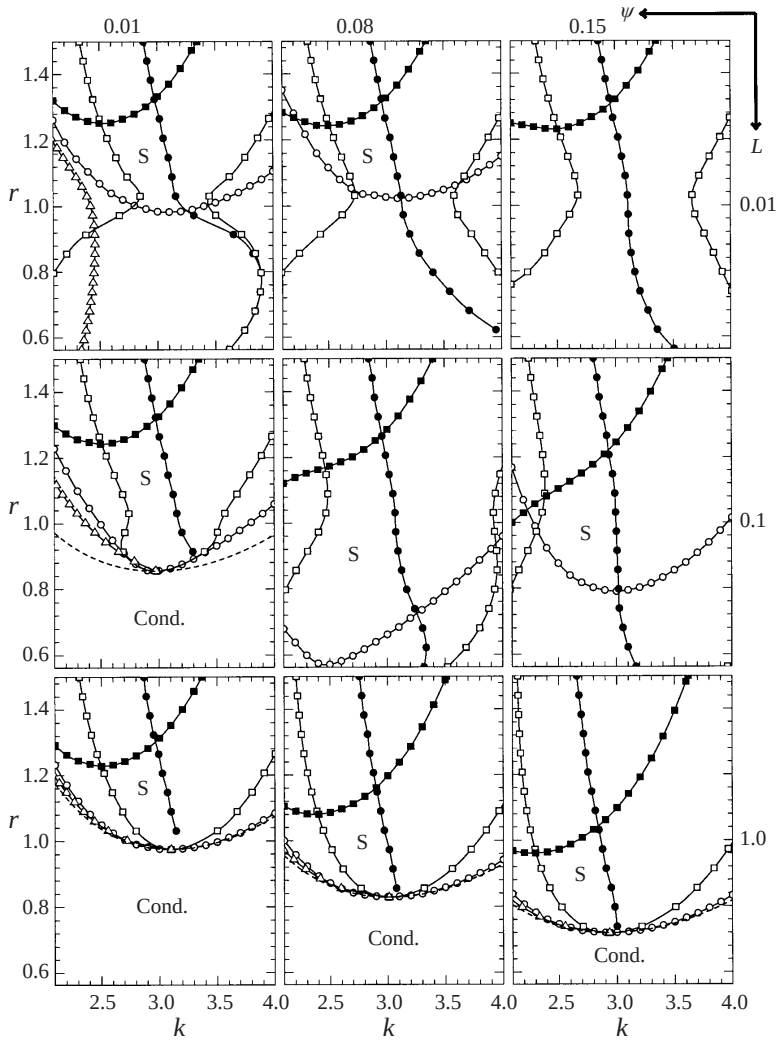

FIGURE 10. Cross-sections of the stability balloon of rolls in the (k, r)-plane at $\sigma = 0.1$. Open circles: CR, open squares: EC, open triangles: ZZ, filled circles: SV, filled squares: OS. S denotes the region of stable rolls. For $\psi = 0.15, L = 0.01$ there are no stable rolls.

and an effective reduced Rayleigh number

$$r_{eff} = \epsilon_{eff} + r^0_{stab}(k). \tag{4.4}$$

Within the amplitude equations $\epsilon_{eff} = \epsilon$. Plotting the EC boundary in the (k, r_{eff})-plane instead of in the (k, r)-plane shows only a dependence on σ but not on ψ and L in the Rayleigh region, cf. figure 14. However, this procedure does not hold in the Soret region.

4.3. *Stability boundaries of squares*

Performing the stability analysis of squares we had to restrict ourselves to the case $d = b = 0$ where the perturbations separate into different symmetry classes. An analytical investigation of long-wavelength perturbations of squares near the critical point can be found in Hoyle (1993). Because both squares and rolls can be described

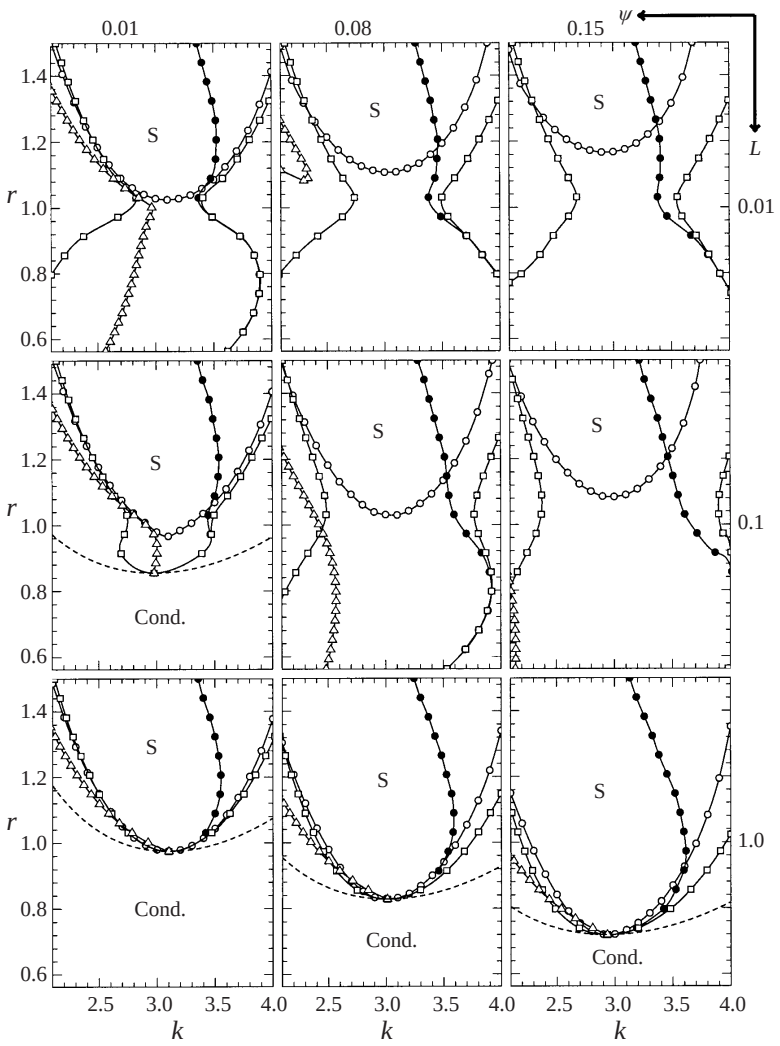

FIGURE 11. As figure 10 but at $\sigma = 1$.

as even in x and y and as mirror glide antisymmetric, one expects a perturbation that destabilizes the squares and favours the rolls to fulfil these symmetries, too. However such a perturbation should break the symmetry $x \leftrightarrow y$. We actually always found the most critical perturbation to fall into this symmetry class. Other perturbations that break the mirror symmetry in the x- or y-direction are less critical.

Figure 15 shows typical examples for the stability region of squares. The left- and right-hand sides of the stability boundaries might be not important – presumably square structures are destabilized earlier by instabilities with finite b or d that tune the wavenumber and that are not considered here.

Even if squares are stable at onset they always lose their stability to a roll pattern at higher r. Furthermore, for certain parameters there does also exist a band of r-values where neither squares nor rolls are stable. Within this band three-dimensional crossrolls that break the $x \leftrightarrow y$ symmetry can be stable. For certain parameters we

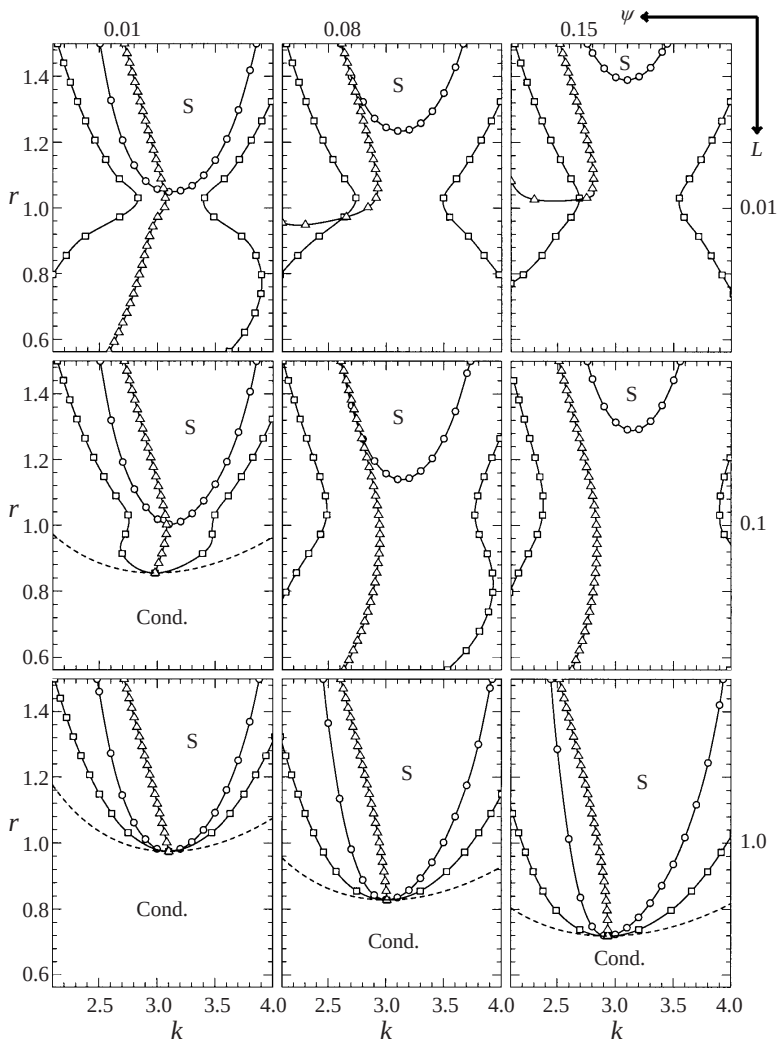

FIGURE 12. As figure 10 but at $\sigma = 10$.

found stationary crossrolls only. For others oscillating crossroll structures appeared as well. We have studied these structures in more detail in Jung *et al.* (1998).

5. Conclusion

We investigated roll, crossroll, and square convection in binary mixtures for a wide range of parameter combinations using a multi-mode Galerkin method. All these patterns are realized as stable convection structures somewhere in parameter space. The bifurcation behaviour of rolls and squares can be modelled near onset by amplitude equations which, however, lose their applicability in the Rayleigh region. Moreover, the crossroll solution that connects the roll and the square branch at Rayleigh numbers $r \approx 1$ is absent in a simple ansatz of cubic amplitude equations.

We compared the Nusselt number and also the mixing parameter of the full numerical solutions for rolls and squares. We found these global properties of the convective

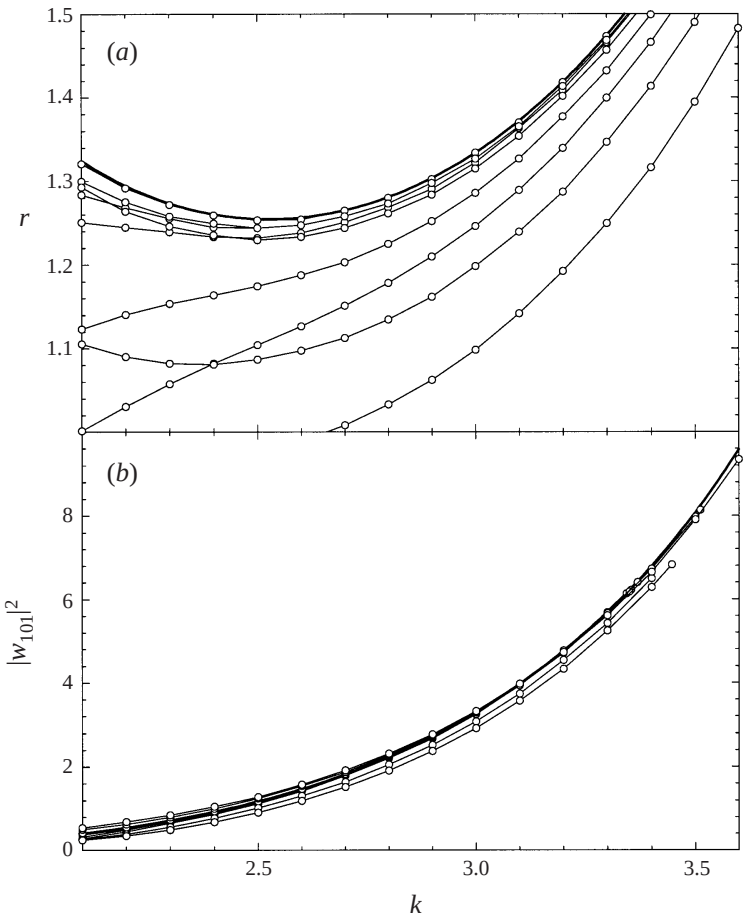

FIGURE 13. (*a*) OS boundaries $r_{OS}(k)$ for the nine parameter combinations of figure 10 versus k. (*b*) Amplitude square $|w_{101}|^2(k)$ of the leading velocity mode of the roll patterns at the OS boundaries shown in (*a*). Thick lines in (*a*) and (*b*) refer to the pure fluid at the same $\sigma = 0.1$.

states to be approximately the same for these patterns despite the qualitatively different structures of the concentration fields of squares and rolls. Rolls show a strong boundary layer behaviour at small L and high r, so that compared to pure fluids much more modes are needed to describe them. Squares, on the other hand, show a less pronounced boundary layer behaviour making it easier to determine these three-dimensional solutions numerically.

In the main part of the paper we investigated the linear stability of rolls and squares. To that end we performed a full and unrestricted stability analysis for rolls using arbitrary perturbations and in addition a stability analysis of squares that uses the periodic boundary conditions of the squares also for the perturbations. The result is that squares are stable in the Soret region if L is sufficiently small. But they always lose their stability at higher r. Rolls are stable at onset at higher L and in the Rayleigh region where squares are unstable. Typically, however, there is a finite interval of r-values in between where neither rolls nor squares are stable. In this interval either stationary or oscillatory crossroll patterns are observed.

The analysis of the rolls shows that in the parameter range explored only the basic

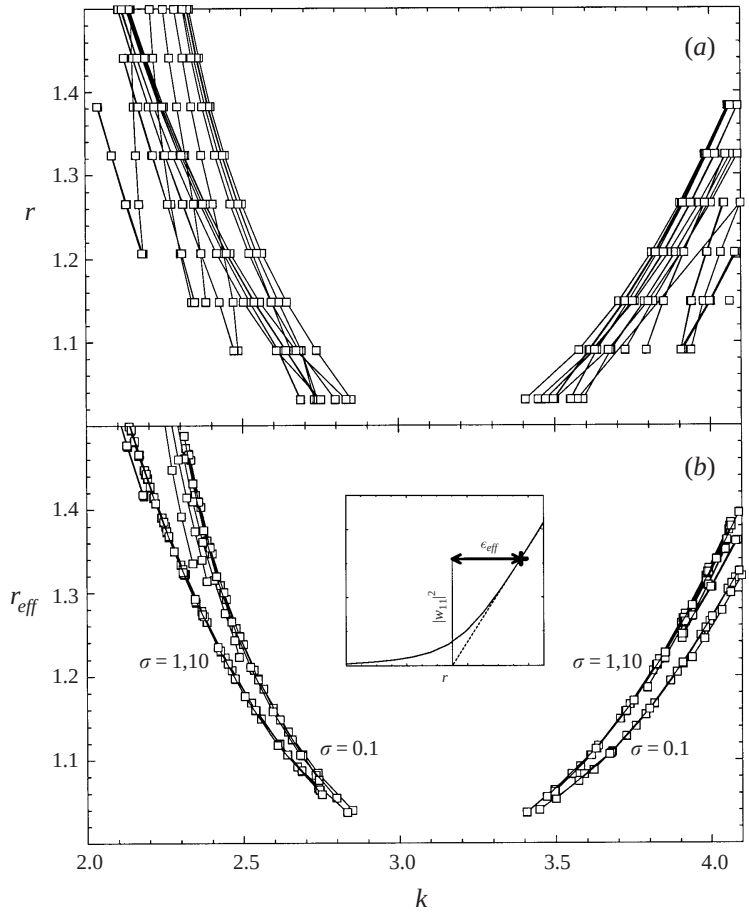

FIGURE 14. (*a*) EC boundaries $r_{EC}(k)$ for the 27 parameter combinations of figures 10–12 versus k. (*b*) EC boundaries of (*a*) in the (k, r_{eff})-plane defined by (4.3), (4.4). Only data $r_{EC}(k) > r^0_{stab}(k)$ in the Rayleigh region are shown. The location of the EC boundary depends only slightly on σ for $\sigma > 1$. Therefore, only two different boundaries appear in (*b*). The inset shows the definition of ϵ_{eff}.

mechanisms of instability occur that are already known from the pure fluid, namely the Eckhaus, zigzag, crossroll, oscillatory, and skewed varicose mechanisms. When the Soret region is small, the stability balloon of the mixtures resembles the Busse balloon for the pure fluid. However, at small L when the Soret region is large the situation is different. The fixed point solutions show a sharp transition between the two regimes. The convection amplitudes are very small in the Soret regime. But near $r = 1$ they increase strongly and e.g. the Nusselt number becomes comparable to that of the pure fluid convection. The stability boundaries of roll convection show a similar transition here. In the Rayleigh region the boundaries are close to the boundaries of the pure fluid. But upon reducing the Rayleigh number the boundaries begin to deviate from their pure fluid counterparts. Near onset they finally agree with the predictions of the amplitude equations for the mixtures.

The EC boundary is a typical example of this behaviour. For high L it has a normal parabolic shape. But for small L one observes a qualitatively different behaviour. When approaching $r = 1$ from above the two branches do not meet near

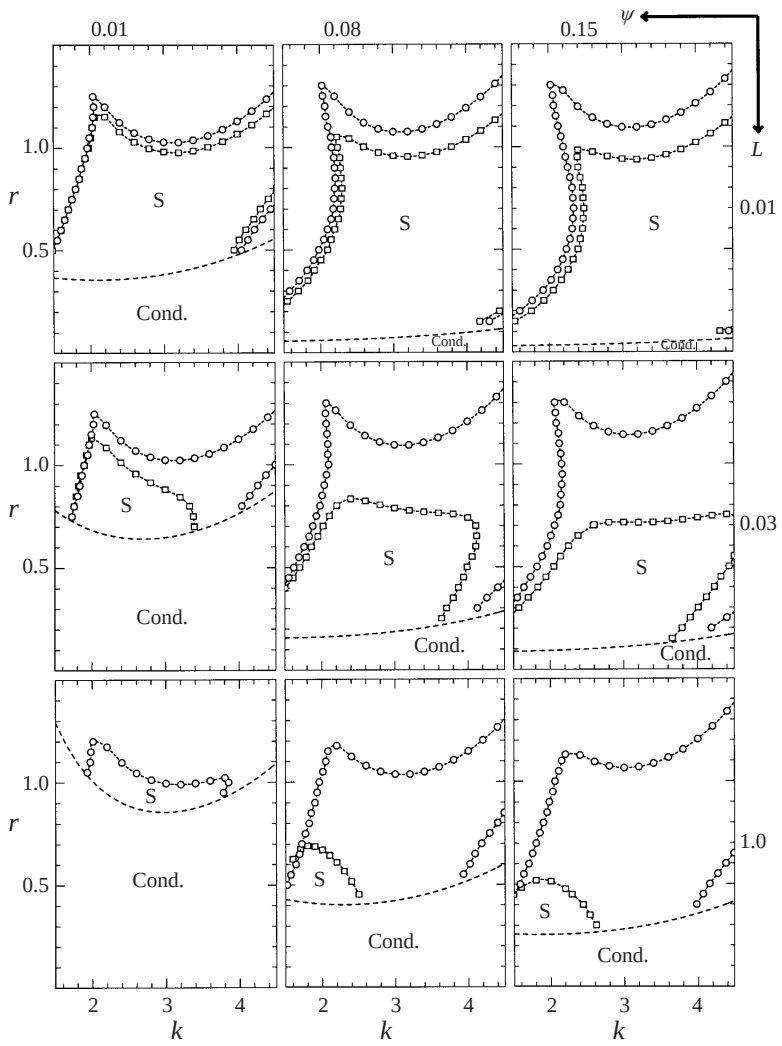

FIGURE 15. Cross-sections of the stability balloon of squares in the (k, r)-plane obtained at $\sigma = 0.1$ (open squares) and $\sigma = 10$ (open circles) from a restricted stability analysis as explained in the text. S denotes the region of stable squares. For $\sigma = 0.1$, $L = 0.1$, and $\psi = 0.01$ there are no stable squares.

$r = 1$ as in the pure fluid but begin to separate again until r gets small enough for the amplitude equations to become valid. A typical vase-like shape results.

A detailed inspection of the point where the rolls become unstable at onset shows that the crossroll boundary is responsible for this loss of stability. As long as the rolls are stable at onset, the crossroll boundary touches the critical point, as predicted by the amplitude equations. At a certain point the amplitude equations show a global loss of stability to crossroll perturbations. In the full Galerkin analysis this loss of stability does not occur. The crossroll boundary disconnects from the neutral curve and the rolls remain stable not at onset but at higher r.

Both the amplitude equations and the full Galerkin expansion show that square structures become stable at onset when roll structures lose stability there and vice

versa. The stability domain of squares lies mainly in the Soret region and it is separated from the region of stable rolls at higher r by the region of crossroll structures. The fact that square patterns have already lost their stability at relatively small r was another favourable property which reduced the requirements for a numerical analysis of these patterns.

The perturbations to which square solutions are unstable show those symmetries that squares, rolls, and crossrolls have in common. But they break the $x \leftrightarrow y$ symmetry, which exists only for squares. The resulting stability boundary delimits the region of stable squares in the (k, r)-plane not only on top but also at the sides at smaller and larger wavenumbers. It should be noted that our analysis of squares does not cover instabilities that retune the actual wavenumber of the pattern considered and which might occur earlier than the wavenumber-preserving instabilities investigated here.

This work was supported by the Deutsche Forschungsgemeinschaft.

REFERENCES

Bolton, E. W., Busse, F. H. & Clever, R. M. 1985 Oscillatory instabilities of convection rolls at intermediate Prandtl numbers. *J. Fluid Mech.* **164**, 469.

Busse, F. H. 1967 On the stability of two-dimensional convection in a layer heated from below. *J. Maths Phys.* **46**, 140.

Busse, F. H. 1978 Non-linear properties of thermal convection. *Rep. Prog. Phys.* **41**, 1929.

Cakmur, R. V., Egolf, D. A., Plapp, B. B. & Bodenschatz, E. 1997 Bistability and competition of spatiotemporal chaotic and fixed point attractors in Rayleigh–Bénard convection. *Phys. Rev. Lett.* **79**, 1853.

Chandrasekhar, S. 1981 *Hydrodynamic and Hydromagnetic Stability*. Dover.

Clever, R. M. & Busse, F. H. 1989 Three-dimensional knot convection in a layer heated from below. *J. Fluid Mech.* **198**, 345.

Clever, R. M. & Busse, F. H. 1990 Convection at very low Prandtl numbers. *Phys. Fluids* A **2**, 334.

Clever, R. M. & Busse, F. H. 1991 Instabilities of longitudinal rolls in the presence of Poiseuille flow. *J. Fluid Mech.* **229**, 517.

Clune, T. & Knobloch, E. 1991 Square pattern convection in binary fluids with realistic boundary conditions. *Phys. Rev.* A **44**, 8084.

Clune, T. & Knobloch, E. 1992 Mean flow suppression by endwalls in oscillatory binary fluid convection. *Physica* D **61**, 106.

Cross, M. C. & Hohenberg, P. C. 1993 Pattern formation outside of equilibrium. *Rev. Mod. Phys.* **49**, 581.

Hollinger, St. 1996 Theorie der ausgedehnten stationären und wandernden Konvektion in binären Fluidmischungen. PhD thesis, Universität des Saarlandes, Saarbrücken.

Hollinger, St. & Lücke, M. 1995 Influence of the Dufour effect on convection in binary gas mixtures. *Phys. Rev.* E **52**, 642.

Hollinger, St. & Lücke, M. 1998 Influence of the Soret effect on convection of binary fluids. *Phys. Rev.* E **57**, 4238.

Hort, W., Linz, S. J. & Lücke, M. 1992 Onset of convection in binary gas mixtures: Role of the Dufour effect. *Phys. Rev.* A **45**, 3737.

Hoyle, R. B. 1993 Long wavelength instabilities of square patterns. *Physica* D **67**, 198.

Jung, Ch., Huke, B. & Lücke, M. 1998 Subharmonic bifurcation cascade of pattern oscillations caused by winding number increasing entrainment. *Phys. Rev. Lett.* **81**, 3651.

Knobloch, E. & Moore, D. R. 1988 Linear stability of experimental Soret convection. *Phys. Rev.* A **37**, 860.

Landau, L. D. & Lifshitz, M. E. 1966 *Hydrodynamik*. Akademie-Verlag.

Liu, J. L. & Ahlers, G. 1996 Spiral-defect chaos in Rayleigh-Bénard convection with small Prandtl numbers. *Phys. Rev. Lett.* **77**, 3126.

Liu, J. L. & Ahlers, G. 1997 Rayleigh–Bénard convection in binary gas mixtures: 1. Thermophysical properties and the onset of convection. *Phys. Rev.* E **55**, 6950.

Lücke, M., Barten, W., Büchel, P., Fütterer, C., Hollinger, St. & Jung, Ch. 1998 Pattern formation in binary fluid convection and in systems with throughflow. In *Evolution of Spontaneous Structures in Continuous Systems* (ed. F. H. Busse & S. C. Müller). Lecture Notes in Physics vol. 55, p. 127. Springer.

Moore, D. R., Weiss, N. O. & Wilkins, J. M. 1991 Asymmetric oscillations in thermosolutal convection. *J. Fluid Mech.* **233**, 561.

Moses, E. & Steinberg, V. 1991 Stationary convection in a binary mixture. *Phys. Rev.* A **43**, 707.

Müller, H.-W. & Lücke, M. 1988 Competition between roll and square convection patterns in binary mixtures. *Phys. Rev.* A **38**, 2965.

Platten, J. K. & Legros, J. C. 1984 *Convection in Liquids*. Springer.